Development of EGFR Targeted Nanoemulsion for Imaging and Novel Platinum Therapy of Ovarian Cancer

Srinivas Ganta[1], **Amit Singh**[2], **Niravkumar R. Patel**[1], **Joseph Cacaccio**[3], **Yashesh H. Rawal**[3], **Barbara J. Davis**[1], **Mansoor M. Amiji**[2,4], and **Timothy P. Coleman**[1,3,4,5]

[1]Nemucore Medical Innovations, Inc., Worcester, MA 01608

[2]Department of Pharmaceutical Sciences, School of Pharmacy, Northeastern University, Boston, MA 02115

[3]Blue Ocean Biomanufacturing, Inc., Worcester, MA 01608

[4]Center for Translational Cancer Nanomedicine Northeastern University, Boston, MA 02115

[5]Foundation for the Advancement of Personalized Medicine Manufacturing, Phoenix, AZ 85013

Abstract

Purpose—Platinum-based chemotherapy is the treatment of choice for malignant epithelial ovarian cancers, but generalized toxicity and platinum resistance limits its use. Theranostic nanoemulsion with a novel platinum prodrug, myrisplatin, and the pro-apoptotic agent, C_6-ceramide, were designed to overcome these limitations.

Methods—The nanoemulsions, including ones with an EGFR binding peptide and gadolinium, were made using generally regarded as safe grade excipients and a high shear microfluidization process. Efficacy was evaluated in ovarian cancer cells, SKOV3, A2780 and A2780$_{CP}$.

Results—The nanoemulsion with particle size <150 nm were stable in plasma and parenteral fluids for 24 h. Ovarian cancer cells *in vitro* efficiently took up the non-targeted and EGFR-targeted nanoemulsions; improved cytotoxicity was observed for the these nanoemulsions with the latter showing a 50-fold drop in the IC$_{50}$ in SKOV3 cells as compared to cisplatin alone. The addition of gadolinium did not affect cell viability *in vitro*, but showed relaxation times comparable to Magnevist®.

Conclusion—The myrisplatin/C_6-ceramide nanoemulsion synergistically enhanced *in vitro* cytotoxicity. An EGFR binding peptide addition further increased *in vitro* cytotoxicity in EGFR positive cancer cells. The diagnostic version showed MR imaging similar to the clinically relevant Magnevist® and may be suitable as a theranostic for ovarian cancer.

Keywords

C_6-ceramide; EGFR; gadolinium; MRI; nanoemulsion; ovarian cancer; platinum

All correspondence should be addressed to: Timothy P. Coleman, PhD, CEO & President, Nemucore Medical Innovations, Inc., Worcester, MA 01608, tcoleman@nemucore.com.

1. INTRODUCTION

Platinum (Pt)-based chemotherapeutics are frontline therapy for a broad range of cancers. For ovarian cancer, Pt-based drugs - carboplatin and cisplatin - increase overall survival and tumor free survival better than any other chemotherapeutic drug (1). Pt containing compounds are alkylating agents that exert anticancer activity by disrupting DNA structure in cell nuclei through the formation of intrastrand and interstrand cross-links (2-4). This mechanism of action not only accounts for the Pt based drug killing of proliferating cancer cells but also accounts for the severe damage to normal cells and thus generalized toxicity.

Ovarian cancer, as well as other cancer types, also develop resistance to Pt-based therapies through multiple mechanisms including increasing membrane pumps to reduce the intracellular drug concentration, inducing enzymes to inactivate the drug, or enable DNA repair pathways to overcome Pt alkylation. For recurrent ovarian cancer, treatment decisions are based on a cancer being "Pt-sensitive" or "Pt-resistant" underscoring the central role that Pt chemotherapy has in the treatment of this disease.

Nanomedicines can be engineered with attributes for mitigating the Pt-based chemotherapy limitations of toxicity and resistance through many strategies. For example, lipoplatin, a liposomal cisplatin, reduces tumor burden comparable to cisplatin but has an improved toxicity profile because of the slower release and lower exposure of Pt to normal tissues (5). However, the ability to encapsulate and control release of Pt-based derivatives in nanomedicines is challenging because of the physicochemical properties of Pt. One physicochemical parameter used for the design of Pt-based drugs, lipophilicity, is critical for encapsulation in nanoparticulate delivery systems and improved transport through biological membranes (6,7). Recently, a safer and more effective platinum (IV) prodrug was synthesized with enough hydrophobicity to allow for encapsulation in PLGA-b-PEG nanoparticles (7). Such modifications allow manipulation of Pt chemistry to incorporate Pt into nanoemulsion formulations as drug payload.

We previously showed the utility and flexibility of nanoemulsion formulations to improve chemotherapeutic delivery and efficacy for ovarian cancer (8-10). Nanoemulsions are colloidal carriers formed by dispersion of oils in water and stabilized with an amphiphilic phospholipid monolayer (9-15). Generally these systems can incorporate significant amounts of hydrophobic drug in the high volume fraction of the oil core (9-13,15). Additionally, they are composed entirely of generally regarded as safe grade (GRAS) materials, which have highly favorable safety profiles. With a size less than 200 nm, nanoemulsions can preferentially enter cancerous tissue via the enhanced permeability and retention (EPR) effect. With a modifiable lipid surface, targeting ligands can be added to assist transport of the nanoemulsion into cancer cells via endocytosis. Once in the cell the GRAS-grade biopolymers used to construct the nanoemulsion are degraded and the encapsulated payload is released. Thus, nanoemulsion drug delivery has several useful features that could provide protection and targeted delivery of Pt-based chemotherapy.

We describe herein the development of a nanoemulsion (NE) with an improved lipophilic Pt-conjugate, the addition of a chemopotentiator, an ovarian cancer targeting molecule and

an imaging agent as the initial step in improving Pt-based chemotherapy for ovarian cancer patients.

2. MATERIALS AND METHODS

2.1 Materials

Cisplatin (*cis*-diammineplatinum (II) dichloride), 2,7-bis(*o*-arsenophenylazo)-1,8-dihydroxynaphthalene-3,6-disulfonic acid (arsenazo III), diethylenetriaminepentaacetic dianhydride (DTPA), 3-[4,5-dimethyl thiazolyl]-2,5-diphenyl tetrazolium bromide (MTT reagent), gadolinium (III) chloride ($GdCl_3$) hexahydrate and sodium myristic acid were from Sigma Chemicals (St. Louis, MO). N-hexanoyl-D-erythro-sphingosine (C_6-ceramide), L-α-phosphatidylethanolamine transphosphatidylated (PE) and 1,2-dioleoyl-*sn*-glycero-3-phosphoethanolamine-N-(lissamine rhodamine B sulfonyl) (Rh-PE) were from Avanti Polar Lipids (Alabaster, AL). Egg phosphotidylcholine (Lipoid® E80) was from Lipoid GmbH (Ludwigshaffen, Germany). Slowfade® Gold Antifade reagent supplemented with nuclear stain DAPI was from Life Technologies. The pegylating agent, methoxy-poly(ethylene glycol)-2000 distearoyl-sn-glycero-3-phosphoethanolamine, sodium salt ($PEG_{2000}DSPE$) was from Lysan Bio, Inc. (Arab, AL). Poly unsaturated fatty acid (PUFA) rich flax seed oil was from Puritan's Pride, Inc. (Oakdale, NY). Dialysis bags with the molecular weight cut-off of 3500 Da and 6-8000 Da were obtained from Spectrum Laboratories, Inc. (Rancho Dominguer, CA). All other chemicals and solvents used were of the highest available grade.

2.2 Synthesis of components

2.2.1 Synthesis of the hydrophobic platinum derivative—Hydrophobic platinum monomyristate (myrisplatin) used in this study was prepared by a revised synthetic route (16). Cisplatin was used as the starting material. Cisplatin (240 mg) was suspended in 30 ml of distilled water and heated to 70°C to form a solution. Silver nitrate (135.9 mg) in 10 ml of water was added drop-wise to the cisplatin solution at room temperature and was stirred for 3 h under light shielding conditions. The resulting white precipitate was separated by filtration. The filtrate was reacted with sodium myristic acid (200 mg) dissolved in 10 ml of water, and stirred at room temperature for 3 weeks to complete the reaction. The translucent white precipitate was filtered, washed with water and ether, and dried in a vacuum chamber. The crude product was then suspended in chloroform, and the soluble fraction was collected and vacuum dried to obtain the myrisplatin. The myrisplatin structure was confirmed by NMR and RAMAN analysis; while the platinum (Pt) content in the sample was determined by Inductively Coupled Plasma-Mass Spectrometry (ICP-MS).

2.2.2 Synthesis of the lipidated EGFR binding peptide—Synthetic endothelial growth factor receptor binding peptide ($EGFR_{bp}$), YHWYGYTPQNVI**GGGGC** with the linker sequence shown in **bold,** was obtained from Tufts University Core Facility (Boston, MA). To make the $EGFR_{bp}$ peptide suitable for incorporation into a nanoemulsion, the peptide was added to MAL-$PEG_{2000}DSPE$ dissolved in HEPES buffer (pH 7.4) at 1:1 molar ratio while mixing under nitrogen at 4°C for 24 h. The resulting $EGFR_{bp}$-$PEG_{2000}DSPE$ conjugate was purified by dialysis (3500 Da) against deionized distilled water, lyophilized and characterized by NMR. Unconjugated $EGFR_{bp}$ in the dialysate was measured using an

RP-HPLC method to determine the concentration of $EGFR_{bp}$ in the $EGFR_{bp}$-$PEG_{2000}DSPE$ conjugate. Briefly, a Hypersil gold C-18 column (4.0×150 mm, 5 µm, Thermo Scientific) was used with a mobile phase consisting of 0.1% trifluoroacetic acid in 10% acetonitrile-water (eluent A) and 0.085% triflouoroacetic acid in 70% acetonitrile-water (eluent B). The eluent gradient was set from 100% to 20% A in 10 min and 20% to 60% A in 5 min, and subsequently back to 100% A over 5 min. The flow rate was 1 ml/min and eluent was monitored at 214 nm for detection of $EGFR_{bp}$.

2.2.3 Synthesis of the lipidated Gd chelate—Lipidated gadolinium (Gd) chelate (Gd-DTPA-PE) was incorporated into nanoemulsion formulations in order to obtain an imaging functionality useful for MRI. Gd-DTPA-PE was synthesized with modifications (17,18). Phosphatidylethanolamine (100 mg) in chloroform (4 ml) with triethylamine (30 µl) was added drop-wise to DTPA (400 mg) dissolved in DMSO (20 ml). The mixture was stirred for 3 h under a nitrogen atmosphere at room temperature. Chloroform was removed by Rota evaporator, and the resulting DTPA-PE conjugate was purified by dialysis (6-8000 Da, Spectrapore, Spectrum Laboratories, CA) against 5% DMSO-water at room temperature for 24 h followed by another 24 h of dialysis in water. The purified sample was then freeze-dried for 48 h. The purity of the DTPA-PE complex was determined by thin layer chromatography (TLC) using a mobile phase of chloroform, methanol and water at 65:25:4 (v/v) ratio, and ninhydrin as the visualizing reagent. In the next step Gd was anchored to the DTPA chelate by adding 18.5 mg of $GdCl_3$ to the DTPA-PE complex in 20 ml of DMSO and the reaction mixture was stirred for 1 h. The resulting Gd-DTPA-PE conjugate was purified by dialysis against water at room temperature for 24 h. The purified sample was freeze dried and stored at -20°C until use.

2.3 Formulation of theranostic nanoemulsions

Nanoemulsion formulations encapsulating myrisplatin and C_6-ceramide in its lipid core with PEG, Gd^{3+} and $EGFR_{bp}$ on the surface were prepared by a high shear homogenization method using a lab scale LV1 Microfluidizer (Microfluidcis Corporation, Newton, MA). The aqueous component of the nanoemulsion formulation was prepared by dissolving egg lecithin (2.4% w/v) and $PEG_{2000}DSPE$ (0.3% w/v) in 4 ml of glycerol (2.21% w/v)-water. Gd-DTPA-PE (2% w/v) and lipidated $EGFR_{bp}$ (0.1% w/v) were then added and stirred for 1 h to achieve complete dissolution of all components. The oil component was prepared by mixing of flax seed oil with the desired amounts of myrisplatin and ceramide dissolved in chloroform, and evaporating the solvent using nitrogen gas. The aqueous and oil components were heated (60°C, 2 min), mixed and then homogenized at 25,000 psi for 10 cycles to obtain the nanoemulsion formulations. Single agent nanoemulsions consisting of either myrisplatin or C_6-ceramide, and corresponding blank nanoemulsions without drug were prepared using a similar process.

2.4 Characterization of the Nanoemulsion Formulation

2.4.1 Particle size and zeta potential analysis—Particle size distribution of the nanoemulsions was determined with the dynamic light scattering (DLS) method using Zetasizer ZS (Malvern, UK). Samples were diluted 1,000 times in deionized distilled water, and the nanoemulsion size (% intensity) was determined at a 90° angle and at 25°C using a

refractive index of 1.45. The polydispersity index (PDI) was used for calculating the particle size distribution. The zeta potential value of the nanoemulsion was also determined using a Zetasizer ZS. Nanoemulsion samples diluted in distilled water were placed in an electrophoretic cell and the zeta potential measured based on the electrophoretic mobility of the nanoemulsion droplets.

2.4.2. Transmission electron microscopy—Transmission electron microscopy (TEM) analysis was used to determine the morphology of the nanoemulsions lipid core. The samples were placed on Firmware-coated copper grids (Electron Microscopy Science, Hatfield, PA) and were allowed to air-dry after draining off the excess nanoemulsion using Whatman filter paper. Negative staining was performed using 1% uranyl acetate for 10 min at room temperature and the excess reagent was drained off using Whatman filter paper. The resulting thin film of sample on the copper grid was observed with a JEOL 100-X transmission electron microscope (Peabody, MA).

2.4.3. Platinum Analysis—The platinum (Pt) concentration in samples was determined using Inductively Coupled Plasma-Mass Spectrometry (ICP-MS). For Pt analysis, 1 mg of myrisplatin was dissolved in 0.1 ml of tetrahydrofuran in microwave tubes and 1 ml of acid mixture (0.8 ml HNO_3 and 0.2 ml HCl) was added, weighed and microwaved. For Pt incorporated into a nanoemulsion, 0.1 ml of sample was transferred to microwave tubes and 0.8 ml of acid mixture (0.5 ml HNO_3 and 0.3 ml HCl) was added. The weights of digest were recorded and diluted to 50 ml in water. All samples were further diluted prior to analysis in 1.5% HNO_3 and 4% HCl. The analysis was performed using an Inductively Coupled Plasma-Mass Spectrometry (ICP-MS) (Agilent 7500cx series ICP-MS). Pt concentration in each sample was calculated using a Pt calibration (1-50 ng/g) curve prepared from a NIST SRM 3140 standard.

2.4.4. Gadolinium assay—A colorimetric assay using arsenazo III was employed to determine free Gd^{3+} during the Gd-DTPA-PE synthesis and also to quantify the free Gd content in the final product and formulations as described previously (19,20). Samples assayed for free Gd were prepared by mixing of a 50 μl sample with 100 μl of 0.2 mM arsenazo III solution and diluted to 1 ml with water. Then 200 μl aliquots of these samples were added to a 96 well plate and read at 652 nm on a Synergy HT plate reader (BioTex). A standard curve of Gd with a linearity range of 2 – 50 μg/ml was prepared using $GdCl_3$ and used to calculate free Gd present in the samples.

2.4.5. T_1 relaxivities—Magnetic resonance imaging (MRI) was used to determine T_1 relaxation times of the Gd containing formulations. Briefly, 0.2 ml of each nanoemulsion sample in tubes was run through a phantom Brucker 500 MHz MRI machine (Bruker Biospec 20/70, Bruker Biospin MRI, Inc, Billerica, MA) in a 4.7 Tesla magnetic field, creating MRI scans showing nanoemulsion generated contrast as well as T_1 time measurements. For comparison Magnevist®, a clinically used Gd-DTPA chelate, was also analyzed for T_1 relaxation time at the same Gd concentration as the Gd-nanoemulsions.

2.4.6. Monitoring of free Pt, Gd and EGFR levels in the formulations—All the nanoemulsion formulations were tested for free Pt, Gd and EGFR$_{bp}$ in the aqueous phase of

formulations using an ultra-filtration method (13). Nanoemulsions were placed in Amicon Ultra centrifugal filter units (3,000 Da, Millipore) and centrifuged at 3,500 rpm for 15 min. The nanoemulsion along with the myrisplatin in the oil phase as well as the surface anchored Gd and EGFR$_{bp}$ conjugates remained in the outer chamber and the aqueous phase moved through the filter into the sample recovery chamber. The concentration of Pt present in the aqueous phase was estimated by a colorimetric assay using *o*-phenylenediamine, and Pt encapsulation efficiency was calculated. Free Gd and EGFR$_{bp}$ present in the aqueous phase were determined by arsenazo III and HPLC assays, respectively, as described above.

2.4.7. Stability of formulations in plasma and intravenous infusions—

Nanoemulsion formulations were diluted in plasma and intravenous infusion solutions, and were monitored for particle size over 24 h at 37°C. The change in particle size as assessed by DLS was used as an indicator of stability upon dilution. For this assay, nanoemulsions were diluted 90% with fresh dog plasma, sodium chloride (0.9%), dextrose (5%) or phosphate buffered saline (PBS pH 7.4) and incubated at 37°C. Aliquots of 10 μl were taken for analysis at 1, 2, 4, 6, 8 and 24 h, diluted 1000-fold with distilled water and analyzed for particle size using a Zetasizer ZS as described above.

2.5 *In vitro* cellular uptake and cytotoxicity studies

2.5.1 Cell Culture Condition—

SKOV3 human ovarian adenocarcinoma cells (ATCC, Manassas, VA) were grown in RPMI medium. A2780 and A2780$_{CP}$ (cisplatin resistant) human ovarian cancer paired cells, generously provided by Dr. Zhenfeng Duan, Massachusetts General Hospital (Boston, MA) were grown in DMEM medium. Both RPMI and DMEM were supplemented with 10% fetal bovine serum and 1% penicillin/ streptomycin. All cell cultures were maintained in a humidified 95% O_2/5% CO_2 atmosphere at 37°C.

2.5.2 Cellular uptake of nanoemulsions—

The cellular uptake of non-targeted and EGFR targeted fluorescent nanoemulsions in SKOV3 cells was investigated by fluorescence microscopy. Rhodamine-labeled nanoemulsions were prepared by loading Rh-PE (0.01% w/v) in a manner similar to the method described in section 2.5. SKOV3 cells were seeded in 6-well plates over cover slips at a density of 100,000 cells/well. After 24 h, cells were incubated for 5, 15, 30 or 60 min with 2 μl of Rh-labeled nanoemulsions diluted with 2 ml of media per well. Cells were then washed with PBS and fixed in 10% formalin for 30 min. The coverslips were inverted onto a glass slide with a drop of Slowfade® Gold Antifade mounting media supplemented with DAPI and incubated for 30 min in the dark. Images were captured to visualize fluorescence using a Zeiss confocal microscope (LSM-700) at 60x magnification.

2.5.3 Cytotoxicity in drug-sensitive and drug-resistance tumor cells—

SKOV3, A2780 and A2780$_{CP}$ cells were seeded at 3000 cells/well in 96-well plates and allowed to adhere overnight. Cells were then treated with cisplatin in PBS, and myrisplatin or ceramide in nanoemulsions at concentrations ranging from 0.01 μM to 100 μM for 72 h. Controls were blank nanoemulsions and vehicles without drug. RPMI or DMEM growth media was used as a negative control and treatment with 0.25 mg/ml poly(ethyleneimine) (10,000 Da), a

cationic cytotoxic polymer, was used as the positive control. After 72 h of treatment, cells were washed with complete media and incubated with 50 μg MTT reagent per well for 3 h. Viable cells reduce the tetrazolium compound into an insoluble formazan dye. Then 150 μL DMSO was added to dissolve the formazan crystals and the plates were read at 570 nm using a Bio-Tek Synergy HT plate reader (Winooski, VT) and the percent cell viability values were determined relative to the negative control after subtracting background values. The treatment producing 50% inhibition of cell viability (IC_{50}) was calculated using GraphPad® Prism 5.

Ceramide's proapoptotic effect on Pt potency was evaluated by treating cells with the myrisplatin and C_6-ceramide combination. Cells were treated with myrisplatin concentration ranging from 0.001 to 50 μM plus concentrations of ceramide ranging from 0.001 to 50 μM for 72 h. The Pt treatment producing a drop in the IC_{50} in presence of ceramide was calculated and the best treatment ratio between Pt and ceramide was determined. Additionally, the combination index (CI) was calculated for combination agents using the classic isobologram equation of Chou and Talalay (21,22), CI = a/A + b/B, where, 'a' is the myrisplatin IC_{50} in combination with CER at concentration 'b', A is the myrisplatin IC_{50} without CER, and B is the CER IC_{50} in the absence of myrisplatin. According to this equation, when the CI < 1, the interaction is synergistic; when the CI = 1, the interaction is additive; and when the CI > 1, the two agents are antagonistic.

3. DATA ANALYSIS

Data are reported as the average and standard deviation. Comparisons between the groups were made using student's t-test and with more than two groups, the ANOVA test was used. Values of $p < 0.05$ were considered statistically significant.

4. RESULTS

4.1 Synthesis and Characterization of Lipophilic Pt and Lipidated Conjugates

A Pt prodrug with the lipophilic characteristics needed for encapsulation in a stable nanoemulsion formulation was designed. Using a two-step aqueous reaction we synthesized myrisplatin as the lipophilic Pt prodrug to be incorporated into the oil core of the long circulating targeted nanoemulsion formulations (Fig 1). NMR and RAMAN analysis confirmed the structure of the lipophilic platinum complex (Fig 1).

An EGFR specific peptide was chosen as the targeting modality for ovarian cancer cells because the EGF receptor is overexpressed in most aggressive ovarian epithelial cancers. We (8,23-26) and others (27,28) have shown that EGFR containing molecules target EGFR-expressing tumors. The EGFR targeting capability was established through the use of a non-mitogenic lipidated-version of the 12 amino acid peptide, designated EGFR$_{bp}$, which shares no homology with human EGF and was isolated from a phage display library (28). The EGFR$_{bp}$-PEG$_{2000}$DSPE conjugate was synthesized by reacting the sulfhydryl (-SH) group of the terminal cysteine of the peptide with the maleimide functional group of the MAL-PEG$_{2000}$DSPE construct. The EGFR-PEG$_{2000}$DSPE conjugate was purified and characterized before being incorporated into the nanoemulsions.

The paramagnetic agent, Gd, was chelated to the DTPA-PE conjugate for incorporation into the nanoemulsion as a contrast enhancement functionality suitable for visualization by MRI. The DTPA-PE complex was synthesized and the complex formation and purity were confirmed by an R_f value of 0.4 using a TLC method (29). In the subsequent step, an arsenazo III assay was employed to monitor the Gd chelation and amount of free Gd binding. The amount of Gd in the conjugate was about 9.8 %w/w. The relaxation time (T_1) of aqueous solution of Gd-DTPA-PE was measured by MRI. Compared to the T_1 of 3,200 msec for plain water, the T_1 of 183 msec for the Gd-DTPA-PE conjugate with 10 mM of Gd confirmed that the Gd retained its magnetic properties in the DTPA-PE complex.

4.2 Formulation and Processing Conditions

A multi-functional theranostic nanoemulsion encapsulating myrisplatin and ceramide was produced using a high shear microfluidization process (Fig 2). The processing conditions (25,000 psi for 10 cycles) were optimized to obtain nanoemulsions with particle size below 150 nm. Higher processing pressure and more cycles did not improve this result as noted previously (12). The lipidic core of the nanoemulsion formulation was flax seed oil, which is rich in omega-3 and omega-6 polyunsaturated fatty acids and solubilizes a significant amount of hydrophobic compound. The amount of myrisplatin and C_6-ceramide in the flax seed oil was approximately 25 mg/g and 50 mg/g, respectively. The main constituents of flax-seed oil that promote solubility of poorly aqueous soluble compounds are linolenic acid (57%), an omega-3 fatty acid, and linoleic acid (17% by weight), an omega-6 fatty acid. In a series of initial experiments, the optimal composition of the nanoemulsion formulations was evaluated with respect to the lipid core, the emulsifier concentration and the particle size (data not shown). Amphiphilic surfactant, egg lecithin, was used as the emulsifier in the nanoemulsion formulation that stabilizes the oil dispersion in water by forming a phospholipid monolayer at the oil-water interface. PEG-modification was employed in the formulation to enhance the circulation time of the formulation in blood. Specifically, $PEG_{2000}DSPE$ was incorporated in the nanoemulsion formulation with its phospholipid component distributed into the phospholipid monolayer and the PEG chains oriented outside the oil core and into the aqueous environment. For high affinity targeting to ovarian cancer cells, lipidated $EGFR_{bp}$ conjugated to PEG-DSPE was stabilized in the oil core with DSPE. Additionally, Gd chelated to DTPA-PE was incorporated into the formulation in order to visualize drug distribution and to monitor disease progression in the clinic. As with the targeting ligand, Gd ions, also reside on the outer surface of the oil core and extend into the aqueous environment. This orientation provides a suitable environment for Gd longitudinal relaxivity and generating contrast for MRI.

4.3. Characterization of Nanoemulsion Formulations

4.3.1 Size distribution, zeta potential and TEM analysis—Particle size distribution and zeta potential values of formulations are summarized in Table I. The average particle size of the blank nanoemulsion was 140 nm. The incorporation of myrisplatin and ceramide into the formulation did not significantly change the hydrodynamic size of the nanoemulsion. The DLS method verified these results (Fig 3). Additionally, the PDI for all the formulations was below 0.1 indicating a narrow size distribution of the nanoemulsions. TEM images of negatively stained nanoemulsions showed that the lipid cores were spherical

and uniform in size (Fig 3). The Zeta potential measurements of the nanoemulsions showed a charge in the range of -49 to -59 mV. Nanoemulsion formulations prepared using myrisplatin and C_6-ceramide alone or Rh-PE exhibited similar size distribution.

4.3.2 Pt, Gd and EGFR$_{bp}$ analysis—Presence of Pt in the formulations was quantitated by ICP-MS at the Nanotechnology Characterization Laboratory and showed that the nanoemulsions contained the expected amount of Pt, ~1 mg/ml. There was no free Pt in the aqueous phase. This high drug encapsulation efficiency of the nanoemulsions was attributed to the relative lipophilicity of the myrisplatin, which was retained in the oil core of the nanoemulsion. In addition, formulations were tested for free Gd and EGFR$_{bp}$ in the aqueous phase of the formulations. There was no free Gd or EGFR$_{bp}$ in the aqueous phase indicating that the Gd-DTPA-PE and EGFR$_{bp}$-PEG$_{2000}$DSPE conjugates remained intact during the manufacturing of the nanoemulsion formulation.

4.3.3 T$_1$ relaxation time—The clinical application of MRI requires organ specific differential contrast for the visualization of disease. Chelates of Gd such as the Gd-DTPA complex generate contrast by increasing the relaxation time of nearby water protons and are used in approximately half of all diagnostic MRI procedures (30). Gd chelated to DTPA-PE was incorporated into the nanoemulsion and its longitudinal relaxivity of water was measured using MRI. The contrast efficiency was comparable to the clinically approved gadopentetate dimeglumine (Magnevist®) contrast agent at a 10 mM Gd concentration (Table II).

4.3.4. Stability of formulations in IV infusions and plasma—The physical stability of the theranostic nanoemulsions in plasma and parenteral infusions was evaluated by measuring the particle size distribution over 24 h (Fig 4). The particle size did not change significantly (P > 0.05) indicating that both non-targeted and EGFR$_{bp}$-targeted formulations were intact and that there was no particle aggregation or disruption in presence of either a high electrolyte concentration or plasma proteins. These data suggest that the theranostic nanoemulsion formulations would be stable *in vivo* in the blood circulation, show longer residence time, and increase tumor accumulation through the EPR effect.

4.4 Cellular Uptake of Fluorescent Labeled Nanoemulsions

Studies with fluorescently labeled nanoemulsions showed that both the non-targeted and EGFR targeted formulations were efficiently taken up by SKOV3 cells. Specifically, EGFR targeted nanoemulsions demonstrated more rapid uptake at 5 and 15 min than the non-targeted nanoemulsions (Fig 5). At 30 min, uptake for both nanoemulsions seemed equivalent. However, EGFR targeted nanoemulsion accumulation appeared to be significantly higher at 60 min than the uptake of the non-targeted nanoemulsion. The observed more rapid uptake and higher accumulation of the EGFR targeted nanoemulsion could be the result of receptor-mediated uptake by SKOV3 cells. These results also indicate the potential advantage of using EGFR as an active targeting moiety for ovarian tumor specific delivery as well as for rapid uptake into tumors.

4.5 Cytotoxicity Screening

The *in vitro* cytotoxicity of cisplatin and the nanoemulsion formulations was compared in SKOV3, A2780 and A2780$_{CP}$ ovarian cancer cell lines (Table III). SKOV3 cells, which express EGFR, showed an intrinsic resistance to the parent drug cisplatin with an IC$_{50}$ of 18 μM. Encapsulation of the novel platinum prodrug, myrisplatin, in a non-targeted nanoemulsion or an EGFR$_{bp}$-targeted nanoemulsion resulted in significant increases in cytotoxicity as compared to cisplatin (3.3-fold and 7.6-fold, respectively). Thus, encapsulation of myrisplatin significantly improved the effectiveness of Pt-based cytotoxicity. The addition of the EGFR$_{bp}$ targeting ligand increased cytotoxicity about 2-fold compared to the non-targeted nanoemulsion in this cell line. A dramatic shift in cytotoxicity occurred with the dual payload of ceramide and myristatin at a 1:5 molar ratio. Indeed, the combination proved to be synergistic (Table IV) and was 39.6-fold more potent than the myrisplatin only nanoemulsion formulation. Moreover, the EGFR$_{bp}$-targeted nanoemulsion (myrisplatin/ceramide NE (T)) was 50.5-fold more potent than cisplatin in SKOV3 cells (Table III). Blank nanoemulsions did not produce any cytotoxicity.

A2780 (cisplatin sensitive) and A2780$_{CP}$ (cisplatin resistant) cell lines, which do not express EGFR, were also used in cytotoxicity assays (Table III). A2780$_{CP}$ cells showed significant resistant to both cisplatin and ceramide; while A2780 cells were much more sensitive. Myrisplatin in the nanoemulsion formulation demonstrated significantly higher cytotoxicity in both A2780 and A2780$_{CP}$ cell lines than cisplatin. Additional data indicated that the nanoemulsion loaded with myrisplatin is much more potent than cisplatin. Overall, the nanoemulsion formulation significantly improved cell kill by myrisplatin/ceramide in cisplatin resistant and sensitive ovarian cancer cell lines. The myrisplatin in nanoemulsion is more potent than cisplatin and the combined myrisplatin/ceramide mitigated platinum resistance in both EGFR-positive SKOV3 or EGFR-negative A2780$_{CP}$ cells.

5. DISCUSSION

Cisplatin is used to treat ovarian cancer patients, but there is significant dose related nephrotoxicity. Carboplatin, which has virtually replaced cisplatin for patient treatment, forms reactive species more slowly than cisplatin and has a much better, but still significant, toxicity profile including renal damage, electrolyte loss, nausea and vomiting. Recently platinum compounds containing a monocarboxylate and O -> Pt complexation resulted in a faster release of DNA reactive adducts comparable to cisplatin (31), and formed the basis for designing some lipophilic Pt derivatives suitable for nanoemulsion encapsulation. In this paper, we report the development of a novel lipophilic platinum containing theranostic nanoemulsion with multiple drug loading, tumor targeting and diagnostic capabilities. The overall design of the nanoemulsion should mitigate nephrotoxicity and be an efficacious platinum therapy for women with advanced and Pt-resistant ovarian cancer.

To maintain the potency of cisplatin, but limit side effects, particularly nephrotoxicity we investigated novel hydrophobic platinum-derivatives that could be sequestered in the lipid core of a stable nanoemulsion. Nanomedicines with a diameter >5nm avoid clearance by the kidney. Therefore our nanoemulsions, which are about 100-200nm in diameter, should provide a suitable system to minimize kidney platinum exposure. With the understanding

that we wanted to maintain a hydration rate similar to cisplatin by creating an O->Pt complexation we developed the methodology to attach a single chain of myristic acid to cisplatin and successfully changed cisplatin's physicochemical properties by making it more lipophilic. The resulting hydrophobic platinum-derivative, myrisplatin, is thus suitable for encapsulation in the lipid core of a nanoemulsion. The high solubility of myrisplatin into the lipid core enabled good encapsulation efficiency.

A second reason for encapsulation of platinum in a nanoemulsion is to design additional features into the delivery system that could assist in mitigating Pt-resistant mechanisms. Mechanisms of Pt-resistance include: reduced platinum influx, increased platinum efflux, escape from apoptosis, sequestration by chemical conjugation, or increased DNA repair (32). The present nanoemulsion is designed to enhance platinum influx by receptor-mediated endocytosis, potentially reduce platinum efflux and diminish escape from apoptosis.

To enhance influx the surface of the nanoemulsion was functionalized with an EGFR$_{bp}$, which preferentially binds with high affinity to the EGF receptor and undergoes receptor-mediated endocytosis of the targeted nanoemulsion. Encapsulation of the prodrug, myrisplatin, in the lipid core of the nanoemulsion protects the platinum from the elemental platinum-efflux mechanisms. Additionally, co-delivery of the pro-apoptotic molecule C$_6$-ceramide mitigates apoptosis escape mechanisms.

Normally clinical diagnosis of efficacy takes a long time to determine, but for patients suffering with advanced ovarian cancer time is critical. A Pt-delivery vehicle that can inform the physician of drug up take by a tumor in a short time and in a non-invasive manner was designed by functionalizing the surface of the nanoemulsion with Gd-DTPA-PE chelate. This design with the chelate-Gd residing on the outer surface of the nanoemulsion provides a suitable environment for Gd longitudinal relaxivity and generates contrast for MRI, thus allowing rapid visualization of drug uptake and potentially quicker monitoring of disease progression in ovarian cancer patients.

Disease specific targeting is important to deliver higher concentrations of chemotherapy to the tumor and should have the added benefit of limiting side effects by minimizing systemic distribution. EGFR is a member of the HER/erb family of receptor tyrosine kinases, and its overexpression is associated negatively with progression-free and overall survival in ovarian cancer (33). In light of the correlation with poor clinical outcome we investigated whether targeting EGFR could enhance *in vitro* potency. EGFR targeting was achieved through the use of a lipidated-version of a 12 amino acid peptide that has demonstrated efficient binding and preferential internalization into EGFR over expressing tumor cells *in vitro*, and tumor xenografts *in vivo* (8,25,27,28). The current study found that EGFR targeting enhanced the potency of myrisplatin as compared to the non-targeted approach.

Non-targeted nanoemulsion formulation created for this study has a size below 150 nm (Table I), and show effective uptake by ovarian cancer cells. Although uptake mechanisms of these nanoemulsion formulations have yet to be studied in detail, in general nanoemulsions fuse with cellular membrane and most likely undergo non-specific transport

via phagocytosis. This passive mechanism improved the potency of myrisplatin when compared to cisplatin *in vitro*. However greater potency was observed when the nanoemulsion was functionalized with $EGFR_{bp}$ to facilitate specific uptake via EGFR mediated endocytosis. Both these mechanisms, i.e. passive lipid membrane fusion or receptor-mediated endocytosis, mitigated Pt-resistance associated with poor Pt-influx into the cell.

The potency of myrisplatin is significantly improved by combining myrisplatin with ceramide in the nanoemulsion formulation. Myrisplatin and ceramide show synergy in cytotoxicity assays either with the EGFR-targeted or non-targeted nanoemulsion formulation. The remarkable increase in potency with this combination should be a benefit to therapy and also limit toxic side effects. For example, less Pt can be loaded with ceramide, which would still achieve the same efficacy as cisplatin alone. Our combination nanoemulsion showed a 50-fold increase in cytotoxicity as compared to cisplatin, a finding that suggests the myrisplatin/ceramide could be reduced 50-fold and still be as effective as cisplatin alone. In such a case, the overall body burden of the toxic drug would be greatly reduced thereby reducing unwanted side effects. Alternatively, the drug loaded nanoemulsion could given less frequently while still achieving good efficacy and reducing the long term chemotherapeutic burden to the body.

Ceramide was chosen as the apoptosis enhancer for several reasons. First, exogenous administration of ceramide augments proapoptotic activity of a number of anticancer agents (8,34,35). Second, one mechanism of tumor apoptosis resistance is depletion of intracellular ceramide. The regulation of ceramide levels involves many enzymes, including ceramide synthase, and glucosylceramide synthase (GCS), which provides a major route for ceramide clearance. Over-expression of GCS is associated with decreased rates of apoptosis in many cancer types (36,37). Replacement of ceramide induces apoptosis via the inhibition of Akt pro-survival pathways, mitochondrial dysfunction and stimulation of caspase activity, ultimately leading to DNA fragmentation (38). While the therapeutic benefits of ceramide seem ideal to enhance the efficacy of chemotherapeutics, there are obstacles in the delivery of ceramide: hydrophobicity, cellular permeability, and metabolic inactivation (39,40). Our nanoemulsion provides a drug delivery system that protects ceramide from systemic enzymatic degradation.

Another key challenge in ovarian cancer diagnosis and therapy is the ability to follow drug pharmacodynamics within the tumor region in real time. The nanoemulsion created for this study was designed as a theranostic capable of simultaneously imaging and targeting drug delivery to EFGR-positive ovarian tumors. The nanoemulsion surface is functionalized with the paramagnetic ion, Gd for MRI contrast enhancement. The nanoemulsion formulations had reduced magnetic relaxation times *in vitro* comparable to clinically relevant Mangevist®. Such a theranostic nanoemulsion allows visualization of the myrisplatin/ceramide pharmacodynamics with the potential to monitor tumor progress. If there is little MRI contrast enhancement in the tumor, clinicians will have the opportunity to adjust the dosing regimens or change therapies if the theranostic nanoemulsion is not effective.

Overall, this study demonstrates that the theranostic properties of a targeted Pt nanomedicine should be advantageous for the treatment of highly aggressive EGFR-positive ovarian cancer. As most ovarian cancers will eventually become Pt-resistant we show that co-delivery of myrisplatin and ceramide has a synergetic potency capable of overcoming Pt-resistance. The diagnostic potential of the nanoemulsion is designed for direct monitoring of nanomedicine uptake and has potential for monitoring disease progression. While further preclinical efficacy, imaging and toxicology investigations are required to confirm these results the medical utility of this novel nanomedicine configuration based on the initial results is promising.

6. CONCLUSIONS

We developed a novel theranostic nanomedicine that co-delivers myrisplatin and ceramide, and shows enhanced cytotoxicity capable of overcoming Pt resistance *in vitro*. The diagnostic capability of the nanomedicine shows magnetic relaxation times similar to the clinically relevant MRI contrast agent Magnevist®. Initial tests indicate that this novel theranostic nanomedicine demonstrates great potential to treat difficult cancers like ovarian cancer. Myrisplatin, a novel platinum product, was designed for encapsulation in the lipid core of the nanoemulsion composed of GRAS grade excipients suitable for parenteral administration. This encapsulation of myrisplatin in a nanoemulsion was more potent than cisplatin in *in vitro* ovarian cancer cytotoxicity assays. Co-delivery of myrisplatin with C_6-ceramide, a pro-apoptotic agent, additionally enhanced the potency of the nanoemulsion formulation and the combination was capable of reversing Pt-resistance in $A2780_{CP}$ ovarian cancer cells. The addition of the targeting ligand $EGFR_{bp}$ further increased potency in an EGFR positive SKOV3 ovarian cancer cell line. The multifunctionality of this novel Pt nanoemulsion formulation demonstrates that clinically relevant capabilities can be designed into nanomedicines and that each design has performance characteristics equal to or better than its current day clinical counterpart. An especially attractive feature of the nanomedicine design is the ability to overcome multiple Pt-resistance mechanisms (e.g. reduced influx, enhanced efflux, and escape from apoptosis). Such a therapeutic should have significant application in the treatment of ovarian cancer as well as other cancers where platinum therapy is the standard of care and patients are at risk of developing Pt-resistant tumors.

Acknowledgments

References

1. Neijt JP, Bokkel Huinink WW, van der Burg ME, van Oosterom AT, Willemse PH, Vermorken JB, et al. Long-term survival in ovarian cancer. Mature data from The Netherlands Joint Study Group for Ovarian Cancer. Eur J Cancer. 1991; 27(11):1367–1372. [PubMed: 1835850]

2. Jamieson ER, Lippard SJ. Structure, Recognition, and Processing of Cisplatin-DNA Adducts. Chem Rev. 1999; 99(9):2467–2498. [PubMed: 11749487]

3. Wong E, Giandomenico CM. Current status of platinum-based antitumor drugs. Chem Rev. 1999; 99(9):2451–2466. [PubMed: 11749486]

4. Wang D, Lippard SJ. Cellular processing of platinum anticancer drugs. Nat Rev Drug Discov. 2005; 4(4):307–320. [PubMed: 15789122]

5. Stathopoulos GP. Liposomal cisplatin: a new cisplatin formulation. Anticancer Drugs. 2010; 21(8): 732–736. [PubMed: 20671511]

6. Cronin MT, Dearden JC, Duffy JC, Edwards R, Manga N, Worth AP, et al. The importance of hydrophobicity and electrophilicity descriptors in mechanistically-based QSARs for toxicological endpoints. SAR QSAR Environ Res. 2002; 13(1):167–176. [PubMed: 12074385]

7. Dhar S, Gu FX, Langer R, Farokhzad OC, Lippard SJ. Targeted delivery of cisplatin to prostate cancer cells by aptamer functionalized Pt(IV) prodrug-PLGA-PEG nanoparticles. Proc Natl Acad Sci U S A. 2008; 105(45):17356–17361. [PubMed: 18978032]

8. Talekar M, Ganta S, Singh A, Amiji M, Kendall J, Denny WA, et al. Phosphatidylinositol 3-kinase inhibitor (PIK75) containing surface functionalized nanoemulsion for enhanced drug delivery, cytotoxicity and pro-apoptotic activity in ovarian cancer cells. Pharm Res. 2012; 29(10):2874–2886. [PubMed: 22653667]

9. Ganta S, Amiji M. Coadministration of paclitaxel and curcumin in nanoemulsion formulations to overcome multidrug resistance in tumor cells. Mol Pharm. 2009; 6(3):928–939. [PubMed: 19278222]

10. Ganta S, Devalapally H, Amiji M. Curcumin enhances oral bioavailability and anti-tumor therapeutic efficacy of paclitaxel upon administration in nanoemulsion formulation. J Pharm Sci. 2010; 99(11):4630–4641. [PubMed: 20845461]

11. Sarker DK. Engineering of nanoemulsions for drug delivery. Curr Drug Deliv. 2005; 2(4):297–310. [PubMed: 16305433]

12. Ganta S, Devalapally H, Baguley BC, Garg S, Amiji M. Microfluidic preparation of chlorambucil nanoemulsion formulations and evaluation of cytotoxicity and pro-apoptotic activity in tumor cells. J Biomed Nanotech. 2008; 4(2):165–173.

13. Ganta S, Paxton JW, Baguley BC, Garg S. Pharmacokinetics and pharmacodynamics of chlorambucil delivered in parenteral emulsion. Int J Pharm. 2008; 360(1-2):115–121. [PubMed: 18508212]

14. Ganta S, Deshpande D, Korde A, Amiji M. A review of multifunctional nanoemulsion systems to overcome oral and CNS drug delivery barriers. Mol Membr Biol. 2010; 27(7):260–273. [PubMed: 20929336]

15. Ganta S, Sharma P, Paxton JW, Baguley BC, Garg S. Pharmacokinetics and pharmacodynamics of chlorambucil delivered in long-circulating nanoemulsion. J Drug Target. 2010; 18(2):125–133. [PubMed: 19728787]

16. Maeda, M.; Sasaki, T., inventors. Sumitomo Pharmaceuticals Company Ltd, assignee. Liposoluble platinum (II) complex and preparation thereof. US 6,613,799 B1. 2003.

17. Levchenko TS, Rammohan R, Lukyanov AN, Whiteman KR, Torchilin VP. Liposome clearance in mice: the effect of a separate and combined presence of surface charge and polymer coating. Int J Pharm. 2002; 240(1-2):95–102. [PubMed: 12062505]

18. Tiwari S, Tan YM, Amiji M. Preparation and in vitro characterization of multifunctional nanoemulsions for simultaneous MR imaging and targeted drug delivery. J Biomed Nanotech. 2006; 2(3-4):3–4.

19. Nagaraja TN, Croxen RL, Panda S, Knight RA, Keenan KA, Brown SL, et al. Application of arsenazo III in the preparation and characterization of an albumin-linked, gadolinium-based macromolecular magnetic resonance contrast agent. J Neurosci Methods. 2006; 157(2):238–45. [PubMed: 16769125]

20. Clogston, JD.; Patri, AK. Characterization of Nanoparticles Intended for Drug Delivery. Springer; 2011. Detecting and Measuring Free Gadolinium in Nanoparticles for MRI Imaging; p. 101-8.

21. Chou TC, Motzer RJ, Tong Y, Bosl GJ. Computerized quantitation of synergism and antagonism of taxol, topotecan, and cisplatin against human teratocarcinoma cell growth: a rational approach to clinical protocol design. J Natl Cancer Inst. 1994; 86(20):1517–1524. [PubMed: 7932806]

22. Chou TC, Talalay P. Quantitative analysis of dose-effect relationships: the combined effects of multiple drugs or enzyme inhibitors. Adv Enzyme Regul. 1984; 22:27–55. [PubMed: 6382953]

23. Milane L, Duan ZF, Amiji M. Pharmacokinetics and biodistribution of lonidamine/paclitaxel loaded, EGFR-targeted nanoparticles in an orthotopic animal model of multi-drug resistant breast cancer. Nanomed. 2011; 7(4):435–444.

24. Milane L, Duan Z, Amiji M. Therapeutic efficacy and safety of paclitaxel/lonidamine loaded EGFR-targeted nanoparticles for the treatment of multi-drug resistant cancer. PLoS One. 2011; 6(9):e24075. [PubMed: 21931642]

25. Milane L, Duan Z, Amiji M. Development of EGFR-targeted polymer blend nanocarriers for combination paclitaxel/lonidamine delivery to treat multi-drug resistance in human breast and ovarian tumor cells. Mol Pharm. 2011; 8(1):185–203. [PubMed: 20942457]

26. Xu J, Amiji M. Therapeutic gene delivery and transfection in human pancreatic cancer cells using epidermal growth factor receptor-targeted gelatin nanoparticles. J Vis Exp. 2012; (59):e3612. [PubMed: 22231028]

27. Song S, Liu D, Peng J, Sun Y, Li Z, Gu JR, et al. Peptide ligand-mediated liposome distribution and targeting to EGFR expressing tumor in vivo. Int J Pharm. 2008; 363(1-2):155–161. [PubMed: 18692120]

28. Li Z, Zhao R, Wu X, Sun Y, Yao M, Li J, et al. Identification and characterization of a novel peptide ligand of epidermal growth factor receptor for targeted delivery of therapeutics. FASEB J. 2005; 19(14):1978–1985. [PubMed: 16319141]

29. Grant CW, Karlik S, Florio E. A liposomal MRI contrast agent: phosphatidylethanolamine-DTPA. Magn Reson Med. 1989; 11(2):236–243. [PubMed: 2779414]

30. Bellin MF. MR contrast agents, the old and the new. Eur J Radiol. 2006; 60(3):314–323. [PubMed: 17005349]

31. Paraskar AS, Soni S, Chin KT, Chaudhuri P, Muto KW, Berkowitz J, et al. Harnessing structure-activity relationship to engineer a cisplatin nanoparticle for enhanced antitumor efficacy. Proc Natl Acad Sci U S A. 2010; 107(28):12435–12440. [PubMed: 20616005]

32. Shen DW, Pouliot LM, Hall MD, Gottesman MM. Cisplatin resistance: a cellular self-defense mechanism resulting from multiple epigenetic and genetic changes. Pharmacol Rev. 2012; 64(3):706–721. [PubMed: 22659329]

33. Lee CM, Shrieve DC, Zempolich KA, Lee RJ, Hammond E, Handrahan DL, et al. Correlation between human epidermal growth factor receptor family (EGFR, HER2, HER3, HER4), phosphorylated Akt (P-Akt), and clinical outcomes after radiation therapy in carcinoma of the cervix. Gynecol Oncol. 2005; 99(2):415–421. [PubMed: 16157365]

34. van Vlerken LE, Duan Z, Seiden MV, Amiji MM. Modulation of intracellular ceramide using polymeric nanoparticles to overcome multidrug resistance in cancer. Cancer Res. 2007; 67(10):4843–4850. [PubMed: 17510414]

35. Devalapally H, Duan Z, Seiden MV, Amiji MM. Paclitaxel and ceramide co-administration in biodegradable polymeric nanoparticulate delivery system to overcome drug resistance in ovarian cancer. Int J Cancer. 2007; 121(8):1830–1838. [PubMed: 17557285]

36. Zhang X, Wu X, Li J, Sun Y, Gao P, Zhang C, et al. MDR1 (multidrug resistence 1) can regulate GCS (glucosylceramide synthase) in breast cancer cells. J Surg Oncol. 2011; 104(5):466–471. [PubMed: 21538359]

37. Swanton C, Marani M, Pardo O, Warne PH, Kelly G, Sahai E, et al. Regulators of mitotic arrest and ceramide metabolism are determinants of sensitivity to paclitaxel and other chemotherapeutic drugs. Cancer Cell. 2007; 11(6):498–512. [PubMed: 17560332]

38. Zhu QY, Wang Z, Ji C, Cheng L, Yang YL, Ren J, et al. C6-ceramide synergistically potentiates the anti-tumor effects of histone deacetylase inhibitors via AKT dephosphorylation and alpha-tubulin hyperacetylation both in vitro and in vivo. Cell Death Dis. 2011; 2:e117. [PubMed: 21368888]

39. Stover TC, Sharma A, Robertson GP, Kester M. Systemic delivery of liposomal short-chain ceramide limits solid tumor growth in murine models of breast adenocarcinoma. Clin Cancer Res. 2005; 11(9):3465–3474. [PubMed: 15867249]

40. Shabbits JA, Mayer LD. Intracellular delivery of ceramide lipids via liposomes enhances apoptosis in vitro. Biochim Biophys Acta. 2003; 1612(1):98–106. [PubMed: 12729935]
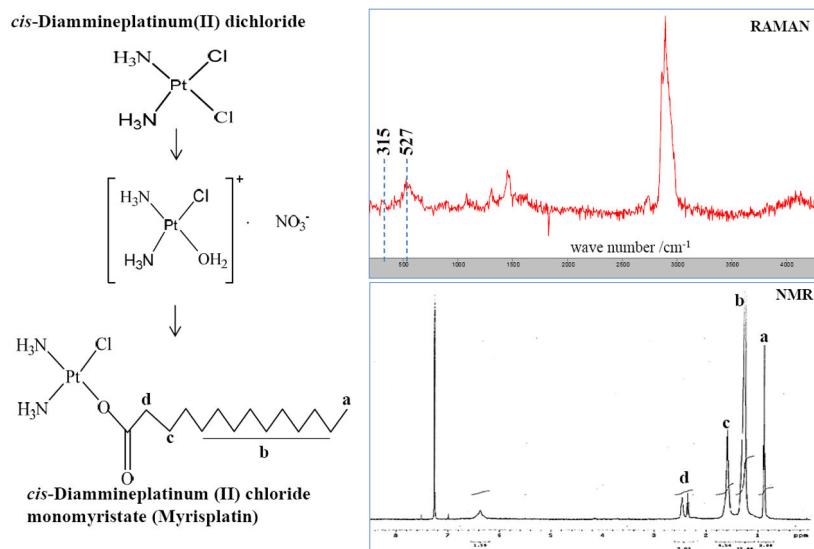
Fig 1.
Scheme of hydrophobic platinum (myrisplatin) formation and structural confirmation using NMR and RAMAN spectra.
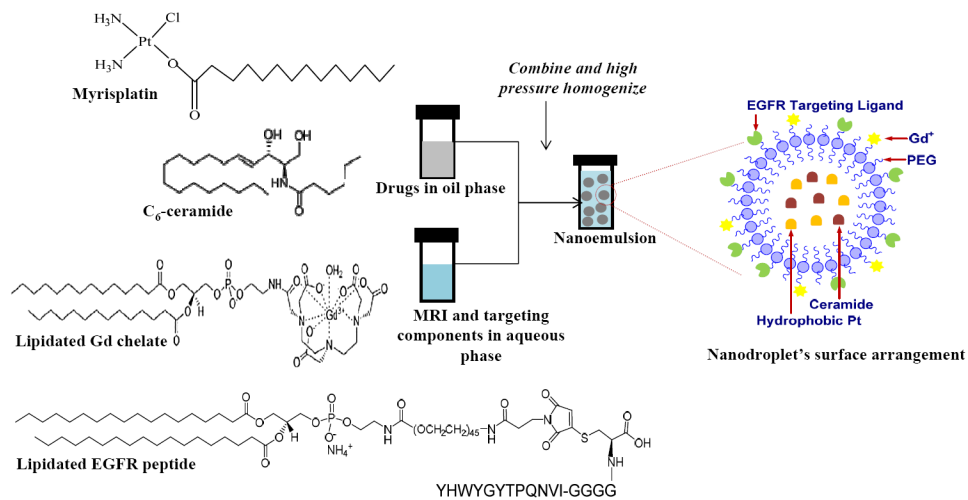
Fig 2.

Schematic showing encapsulation of myrisplatin and C_6-ceramide into lipid core of nanoemulsion and its surface is modified with gadolinium and EGFR binding peptide for MRI functionality and targeting, respectively.
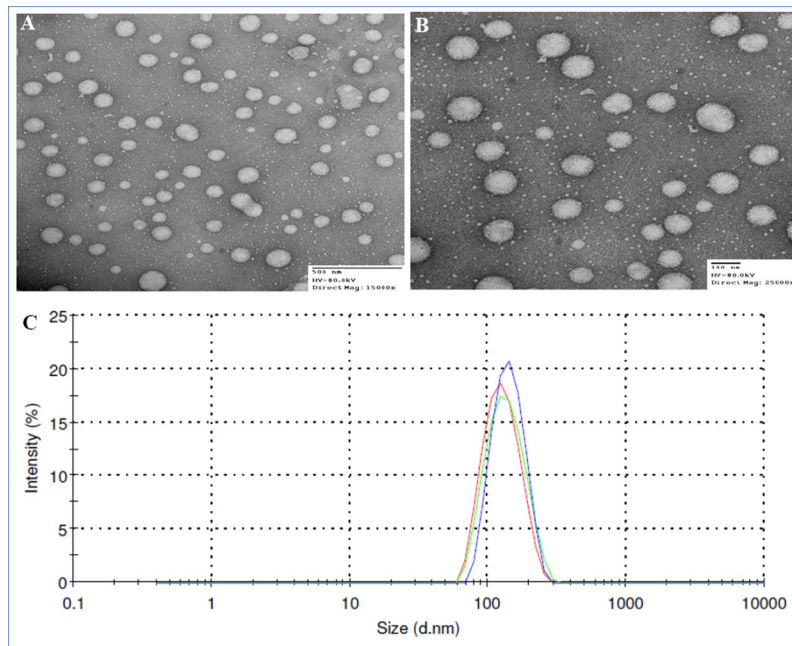
Fig 3.
Transmission electron microscopy images (A. Non-targeted and B. EGFR Targeted) and
size distribution plots (C) of theranostic nanoemulsions produced by high shear
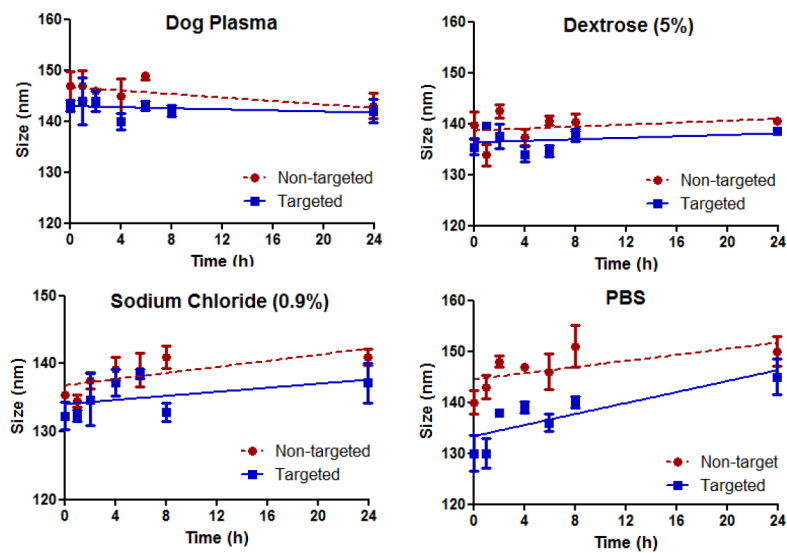microfluidization process using LV1 Microfluidizer.

Fig 4.
Physical stability of formulations upon 90% dilution in plasma, parenteral infusion fluids (5% dextrose and 0.9% sodium chloride) and phosphate buffered saline.
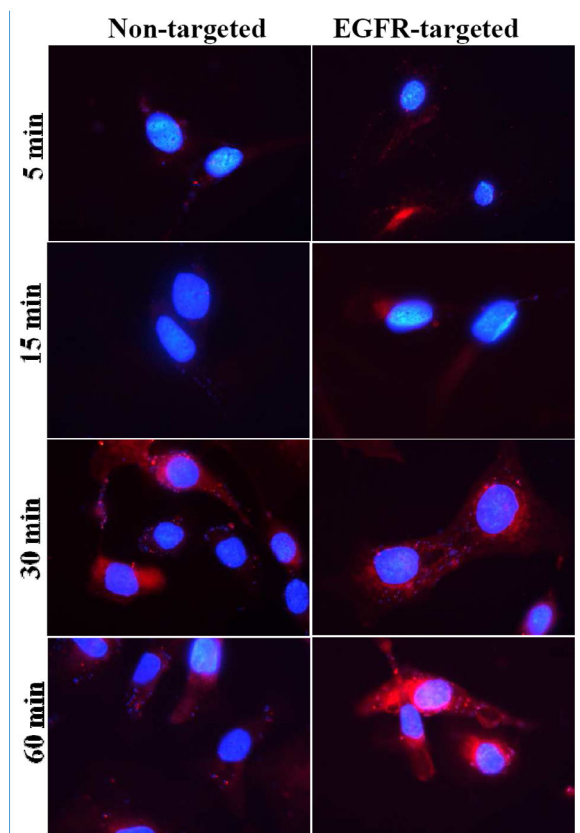
Fig 5.
Fluorescent microscopy images showing uptake of Rh-PE (Red) labeled non-targeted and EGFR targeted nanoemulsions in SKOV3 cells. DAPI (Blue) was used to stain nucleus of SKOV-3 cells. Images were captured using Zeiss confocal microscope (LSM-700) at 60× magnification.

Table I

Characterization of nanoemulsion formulations

Formulations	Hydrodynamic diameter of nanoemulsion droplets		Zeta Potential (mV)	Pt encapsulation efficiency
	Size (nm)	PDI		
Blank nanoemulsion	140 ± 1.6	0.04	-49 ± 10	-
Myrisplatin/ceramide nanoemulsion (non-targeted)	141 ± 3.0	0.10	-54 ± 9	100%
Myrisplatin/ceramide nanoemulsion (EGFR targeted)	146 ± 4.0	0.10	-59 ± 10	100%

The values are shown as Avg ± SD, n=3.

Table II

Estimation of relaxation times (T_1) of gadolinium in nanoemulsions using magnetic resonance imaging

Formulations	T1 relaxivities (msec)
Magnevist® (Gd-DTPA)	22 ± 0.3
Non-targeted Nanoemulsion	35 ± 14
EGFR targeted Nanoemulsion	47 ± 1

Table III

The 50% inhibitory concentration of platinum and C_6-ceramide alone and in combination on ovarian cancer cell lines

Treatment Type	SKOV3	Pt-potency Fold Enhancement	A2780	Pt-potency Fold Enhancement	A2780cp	Pt-potency Fold Enhancement
Cisplatin in PBS	18.2 ± 0.1 μM	--	3.6 ± 0.1 μM	--	96.5 ± 0.1 μM	--
Ceramide in DMSO	10 ± 0.1 μM	--	9.6 ± 0.1 μM	--	30 ± 2 μM	--
Ceramide NE (NT)	9.1 ± 0.1 μM	--	1.5 ± 0.01 μM	--	1.3 ± 0.02 μM	--
Ceramide NE (T)	8.3 ± 0.1 μM	--	ND	ND	ND	--
Myrisplatin NE (NT)	5.5 ± 0.1 μM	3.3	0.24 ± 0.01 μM	15	0.8 ± 0.01 μM	120.6
Myrisplatin NE (T)	2.4 ± 0.1 μM	7.6	0.42 ± 0.01 μM	8.6	ND	ND
Myrisplatin/ceramide NE (NT)	0.46 ± 0.01 μM	39.6	0.16 ± 0.01 μM	22.5	0.4 ± 0.02 μM	241.3
Myrisplatin/ceramide NE (T)	0.36 ± 0.01 μM	50.5	ND	ND	1.1 ± 0.01 μM	87.7

- A2780 & A2780CP cells do not express EGFR, thus IC_{50} not determined (ND) for targeted systems.

- In case of combination treatment, platinum to ceramide molar ratio was 1:5 in the formulation

Table IV

Platinum and ceramide combination index (CI) against SKOV3 ovarian cancer cells

Combination Type	SKOV3	
	CI	Interaction type
Cisplatin/C_6-ceramide	0.46	Synergetic
Myrisplatin/C_6-ceramide NE (NT)	0.86	Synergetic
Myrisplatin/C_6-ceramide NE (T)	0.80	Synergetic

CI<1, synergetic; CI = 1, additive; CI > 1, antagonistic